proceedings

MDPI

Type of the Paper (Proceeding Paper, Abstract, Editorial, etc.)

Defect Detection in Composite Wind Turbine Blade Sandwich Panels Using Dispersion Characteristics of Stress Waves

Chen-Yi Lin[1], Chia-Chi Cheng[1], Yung-Chiang Lin[1], and Jien-Chen Chen[2]

[1] Department of Civil and Construction Engineering, Chaoyang University of Technology, Taichung City 413310, Taiwan;
* Correspondence: s11211616@gm.cyut.edu.tw; ccheng@cyut.edu.tw
† Presented at the "Non-destructive testing and evaluation" in Kobe, Japan, on 15-19 September 2025

Keywords: sandwich composite, wind turbine blade, dispersion, stress waves,dtw

1. Abstract

To detect delamination and internal void defects within sandwich composite ma-terials, such as those used in wind turbine blades, this study employs a Remote Impact Test (RIT), analyzing the dispersion characteristics of the generated stress waves. RITs were conducted on specimens that varied in both thickness and defect type. Time-frequency spectrograms and dispersion curves were then obtained using two time-frequency analysis techniques: wavelet analysis and reassigned spectrograms (derived from Short-Time Fourier Transformation). The accuracy of defect identifica-tion is demonstrably improved through the cross-examination of the findings from these methods.

2. Research Motivation and Methodology

As global reliance on wind energy grows, robust wind turbine operation is essen-tial, with blade integrity being crucial. These composite blades face extreme stresses, leading to hard-to-detect internal defects like delamination, voids, and cracks. Such hidden flaws can drastically reduce efficiency, performance, and lifespan, causing costly repairs and potential catastrophic failures. Therefore, advanced Non-Destructive Testing (NDT) methods are vital for early, reliable subsurface defect detection. This research aims to develop and validate an improved NDT technique to enhance wind turbine blade safety and reliability, thus bolstering sustainable renewa-ble energy. In this study, guided waves are generated using an impact hammer capable of sensing the impact time. An accelerometer is placed at a distance to record the vertical stress wave acceleration. The presence of delamination defects in the composite plates is detected through time-frequency spectrograms derived from wavelet analysis, as well as dispersion curves obtained from short-time Fourier transform (STFT) and the reassigned spectrogram method.

3.Experimental Specimens

The test samples consisted of eleven 40 × 40 cm sandwich composite plates. The internal structure featured a foam core bonded with epoxy resin, sandwiched between upper and lower fiberglass layers. The fiberglass layers were oriented at 90 degrees to each other and stacked in four layers. The surface of each specimen was coated by pro

Citation: To be added by editorial staff during production.

Academic Editor: Firstname Lastname

Published: date

tective paint. The specimen thickness varied depending on the number of foam layers: one, two, or three layers, with each foam layer being 20 mm thick, as shown in Figure 1.Two types of artificial defects were introduced: the first involved saw cuts at the specimen's edge to simulate delamination cracks located either just below the top layer or at the center of the foam core, as illustrated in Figures 1(a) and 1(b). The second type involved creating central void defects of varying lateral dimensions by removing the core material in the center, as shown in Figure 1(c). Table 1 summarizes the specimen IDs, thicknesses, and defect types. Table 1 includes the specifications of each composite panel.

(a) (b) (c)

Figure 1. Damage types in composite sandwich panels: (a) Saw-cut at the upper edge layer(SCU); (b) Saw-cut at the middle of the edge(SCC); (c) Centrally located hollow defect(CV-2、CV-5、CV-15).

Table 1. Identification and Specifications of Composite Panels

Specimen ID (S)	S1	S2-1	S2-2	S3	S4	S5	S6	S7	S8	S9	S10
Specimen Thickness T (mm)	20	40	40	60	40	40	40	40	20	40	60
Defect Type and Location	SCU	SCU	SCC	SCU	SCU	CV-2	CV-5	CV-10	intact	intact	intact

4. Experimental Method

4.1. Equipment Setup

A small impact hammer embedded with piezoelectric material capable of recording the exact time of impact was used to generate stress waves. An accelerometer was placed at a farther location along a horizontally planned measurement line. This test configuration was named as Remote Impact Test (RIT). The received stress wave signals were converted into time-domain waveforms using a AD card.In this experiment, the distance between the impact hammer and the receiver was set to 0.15 m. The data acquisition frequency was 400 kHz, with a total of 8192 data points recorded. The total recording time was 3.276×10^{-3}seconds.

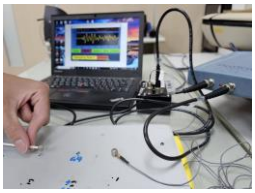

Figure 2. Actual impact testing setup, including a computer,an impact hammer, a accel erometer,an amplifier, and an A/D conversion card.

5. Experimental Results

For the single-layer composite panel S1, Figure 3 displays RIT waveforms for both intact and damaged (SCU) conditions. Damage is identified by changes in oscillating frequencies and amplitudes. Specifically, Figure 3(b) shows that delamination shifts vibrations from high to low frequencies, indicating guided waves within the delami-nated

section. This is followed by a high-amplitude, very low-frequency oscillation, representing the flexural vibration of the upper delaminated layer, contrasting with the intact case (Figure 3(a)). This observation underpins our two subsequent analyses.

The first analysis applied a wavelet transform with a Morlet window [1] to Figure 3's waveforms, generating the time-frequency spectrograms in Figure 4. High-amplitude responses in Figure 4(b) exhibit lower frequencies and occur later than those in Figure 4(a). Initially (under 0.5 ms), a broadband response signifies guided waves arriving above the saw-cut layer.

The second analysis involved suppressing Figure 3's waveforms beyond 0.75 ms (Figures 5(a) and 5(d)) to enhance their initial segment. These modified waveforms were then transformed using Short-Time Fourier Transform (STFT) [2] and the reas-signed method [3] to produce dispersion diagrams (Figures 5(b) and 5(e)). From these, dispersion curves (velocity vs. wavelength) were derived by identifying peak ampli-tudes within successive 50 m/s wave velocity intervals, as seen in Figures 5(c) and 5(d).

We established a baseline using the average dispersion curve from all intact specimens of the same thickness. Then, Dynamic Time Warping (DTW) [4] quantified the similarity between defective curves and this baseline across various velocity ranges to pinpoint the most effective range for distinguishing intact from defective conditions.

For instance, Figures 6(a)-(c) show DTW boxplots for intact S1 (S1-G), intact S8 (S8-G), and S1's SCU section, respectively. The third quartile of DTW for intact areas (Figures 6(a) and (b)) stayed below 0.25. However, for the SCU section, the first quartile of DTW consistently exceeded 0.45 in the 200-500 m/s, 200-550 m/s, and 200-600 m/s ranges. The 200-500 m/s range showed the smallest boxplot, indicating it provides the most optimal distinction.

(a) (b)

Figure 3. Waveform for specimen S1 as an example: (a) S1-G-T20 (intact); (b) S1-D-T20 (with SCU).

(a) (b)

Figure 4. Time-frequency obtained by wavelet analysis specimen S1 as an example: (a) S1-G-T20 (intact); (b) S1-D-T20 (with SCU).

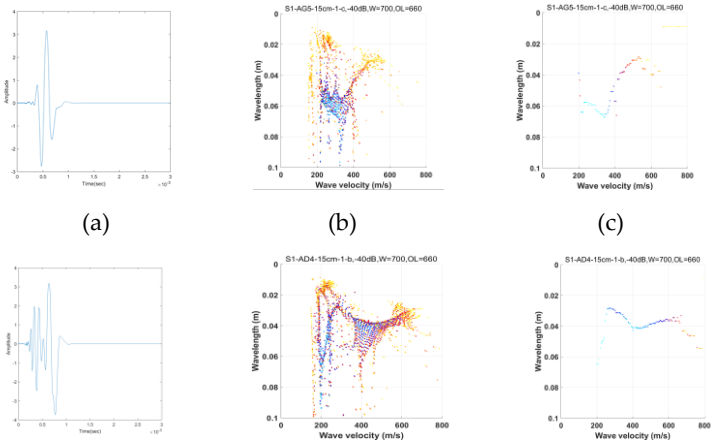

(a) (b) (c)

(d) (e) (f)

Figure 5. Representative results for specimen S1: (a) truncated displacement waveform;(b) Dispersion spectrogram;(c) Dispersion curve for S1-G-T20;(d) truncated displacement waveform for S1-D-T20;(e) Dispersion spectrogram for S1-D-T20, and;(f) Dispersion curve for S1-D-T20.

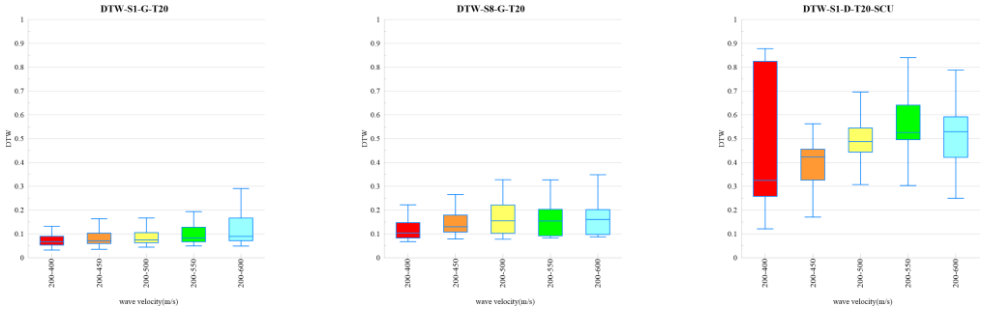

(a) (b) (c)

Figure 6. DTW data analysis results: (a) Boxplot comparison of intact specimens S1-G-T20; (b) Boxplot comparison of intact specimens S8-G-T20;(c) Boxplot comparison of defective specimen S1-D-T20-SCU

6. Conclusion

The time-frequency spectrograms derived from wavelet transform reveal L-shaped features and delayed low-frequency responses in damaged regions. Furthermore, dispersion curves obtained through Short-Time Fourier Transform (STFT) and the reassigned method effectively illustrate the relationship between wave velocity and wavelength, enabling the identification of various defect types and positions.Comparative analysis across specimens with different thicknesses and defect configurations confirms that in the wavelength range below 0.1 meters, solid and defective plates show clear differences in wave speed distribution. Additionally, the method proved capable of detecting central voids with diameters exceeding 50 mm. The integration of Dynamic Time Warping (DTW) to quantify the similarity between dispersion curves further enhances the precision of defect assessment. Statistical analysis of DTW results indicates that for specimens with a thickness of 20 mm, the wave velocity range between 200 and 500 m/s provides the most effective distinction between intact and damaged conditions. This range exhibits the smallest boxplot spread, indicating the best identification performance. For the 40 mm thick SCU specimen, damage could be identified within the wave velocity range of 200 to 550 m/s. The 40 mm thick SCC specimen also exhibited identifiable damage within the 200 to 550 m/s range. In contrast, the 40 mm thick CV-2 specimen did not show a clear indication of damage. However, damage in the CV-5 specimen was identifiable within the 200 to 500 m/s range, while the CV-10 specimen showed detectable damage within the 200 to 550 m/s range. Finally, for the 60 mm thick SCU specimen, damage was distinguishable within the wave velocity range of 200 to 550 m/s.

References

1. Grossmann, A.; Morlet, J. Decomposition of Hardy functions into square integrable wavelets of constant shape. SIAM J. Math. Anal. 1984, 15, 723–736.
2. Allen, J. B. Short term spectral analysis, synthesis, and modification by discrete Fourier transform. IEEE Trans. Acoust. Speech Signal Process. 1977, 25, 235–238.
3. Auger, F.; Flandrin, P. Improving the readability of time-frequency and time-scale representations by the reassignment method. IEEE Trans. Signal Process. 1995, 43, 1068–1089.
4. Sakoe, H.; Chiba, S. Dynamic programming algorithm optimization for spoken word recognition. IEEE Trans. Acoust. Speech Signal Process. 1978, 26, 43–49.